RSC Advances

PAPER

View Article Online
View Journal | View Issue

Cite this: *RSC Adv.*, 2018, **8**, 35700

Ultra-highly fluorescent N doped carbon dots-CdTe QDs nanohybrids with excitation-independent emission in the blue-violet region†

Yuan Jiang,[a] Liang Zheng,[a] Hui Zheng,[a] Feimei Wu,[a] Lihuan Shao,[a] Peng Zheng,[a] Yan Liu *[b] and Yang Zhang *[a]

Received 26th July 2018
Accepted 8th October 2018

DOI: 10.1039/c8ra06326e

rsc.li/rsc-advances

Luminescent carbon dots (CDs) are of significant practical application interest such as in optoelectronic devices and sensitive probing in the life science and environment fields. In this study, N doped CDs-CdTe quantum dots (QDs) nanohybrids (CdTe/N-CDs) were synthesized by a plasma heating process using silk fibroin and CdTe QDs as precursors. The synthesis, doping, hybridizing and passivation of the CdTe/N-CDs were carried out in a single-step process. The as-synthesized CdTe/N-CDs dispersed in ethanol exhibited blue-violet photoluminescence with excitation-independent emission characteristics (strong emissions at 405 nm and 429 nm, and a weak emission at 456 nm). Additionally, the optimal excitation wavelength for the CdTe/N-CDs was found at 360–380 nm, which very closely matches the intrinsic wavelength of GaN-based LEDs. Furthermore, the obtained CdTe/N-CDs exhibited a very high quantum yield of ~84%, showing great potential in developing chip-based high performance optoelectronics devices. The emission mechanism and emission enhancement by related factors including N-bonded configurations in the carbon base and the transfer of photo-excited electrons from the CdTe QDs to the N doped CDs were studied, as well.

Introduction

Carbon-based dots (CDs), which are composed of sp^2 carbon structures and different surface functional groups, are a new kind of carbon nanomaterials that exhibit unique luminescent properties due to quantum confinement and structural edge effects.[1,2] Compared to conventional luminescent semiconductor quantum dots (QDs), CDs have attracted more attention in the fields of optoelectronics,[3,4] biomedical[5,6] and environmental sciences[7,8] for the advantages of robust chemical inertness, low toxicity and good biocompatibility.[9,10] However, most of the CDs reported exhibit a relatively low photoluminescence (PL) quantum yield (QY) (less than 3%), which greatly limits their applications.[11,12]

In the past few years, many efforts have been dedicated to improve the PL QY of CDs through passivation,[13,14] reduction,[15,16] or chemical doping.[17–19] Among these studies, nitrogen doped CDs (N-CDs) exhibit a QY of about 30%, which can be attributed to the strong valence bonds between nitrogen and carbon atoms. Therefore, they are considered as one of the most promising types of CDs for optoelectronics device applications.[20] Alternatively, it has been shown that constructing a hybrid structure with other semiconductor QDs is another efficient strategy to tune the optical and electrical properties of CDs. High QYs up to 78% have been obtained in CDs coated with ZnS, ZnO, and TiO_2.[21,22] However, despite being an important form of semiconductor QDs with high QY, CdTe QDs are rarely reported to be hybridized with CDs.[23,24]

In this work, a novel type of N doped CDs-CdTe QDs hybrid (CdTe/N-CDs) was designed and fabricated. Synthesis was carried out *via* a plasma heating process with a mixture of silk fibroin and CdTe QDs as precursors. The structural and optical properties were investigated using a number of techniques including X-ray photoelectron spectroscopy (XPS), transmission electron microscopy (TEM), Raman spectroscopy, ultraviolet-visible (UV-vis) absorption, PL and lifetime measurement. The obtained nanocomposites exhibit blue-violet luminescence with a very high QY of 84%. The mechanism of QY enhancement was discussed in detail.

Results and discussion

The determination of the elemental composition and the identification of the chemical states of N and C in the synthesized CdTe/N-CDs were carried out *via* XPS analyses, and the resulting C 1s and N 1s spectra are shown as Fig. 1(a) and (b),

[a]*Lab for Nanoelectronics and NanoDevices, Department of Electronics Information, Hangzhou Dianzi University, Hangzhou, Zhejiang 310018, China. E-mail: yzhang09@hdu.edu.cn*

[b]*Chemistry and Biochemistry Department, California State Polytechnic University-Pomona, CA 91768, USA. E-mail: yanl@cpp.edu*

† Electronic supplementary information (ESI) available. See DOI: 10.1039/c8ra06326e

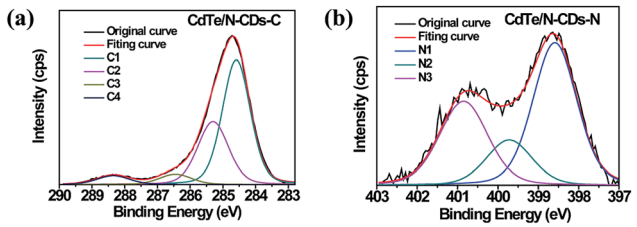

Fig. 1 (a) High-resolution XPS spectrum of C 1s in CdTe/N-CDs. The deconvolution reveals four binding energy peaks centered at C1 (284.8 eV), C2 (285.5 eV), C3 (286.5 eV) and C4 (288.6 eV). (b) High-resolution XPS spectrum of N 1s in CdTe/N-CDs. The deconvolution reveals three binding energy peaks centered at N1 (398.8 eV), N2 (400.0 eV) and N3 (401.0 eV).

respectively. The C 1s spectrum can be deconvoluted into four Gaussian peaks: the C1 peak at 284.8 eV, which is attributed to a pure carbon (C–C bonding) environment, the C2 (285.5 eV) and C3 (286.5 eV) peaks, which are due to the presence of C=N and C–N bonding respectively, and the C4 (288.6 eV) peak, which is attributed to COx.[25] For the N 1s spectrum, three deconvoluted peaks were observed, including pyridinic N1 (398.8 eV), pyrrolic N2 (400.0 eV), and graphitic N3 (401.0 eV).[26–28] Based on these results, it can be deduced that N atoms had been doped into the carbon materials, with an approximate N/C atomic ratio of 8.0 at%.

As illustrated in the TEM images of the obtained CdTe/N-CDs (Fig. 2(a)), some nano-sized particles were distributed uniformly and separated from each other, while others were hybridized into an agglomerate. The isolated particles could be identified as the N-CDs or the CdTe QDs, respectively, by examining the enlarged view of the high-resolution transmission electron microscopy (HRTEM), and the average sizes of both N-CDs and CdTe QDs were about 4.5 nm. Regarding the hybridized particles, two different types of lattice spacing

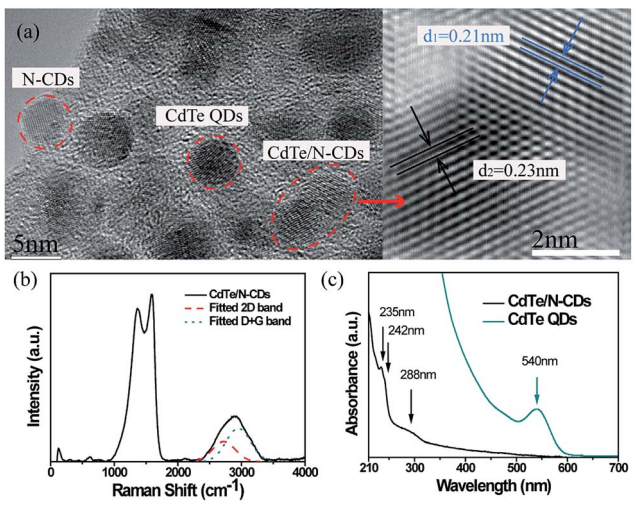

Fig. 2 (a) TEM image of CdTe/N-CDs. Right: magnified image showing the structure of the CdTe/N-CDs. (b) Raman scatting spectra of CdTe/N-CDs, recorded at room temperature. The dashed and dotted lines are fitted 2D and D + G peak curves, respectively. (c) UV-visible absorbance spectra of CdTe/N-CDs and CdTe QDs. The materials were sonicated and dispersed in ethanol.

corresponding to the 0.21 nm of N-CDs (100) planes[29,30] and the 0.23 nm of CdTe QDs (220) planes[31] were observed. Therefore, in these particles, the N-CDs and the CdTe QDs were combined tightly as a whole.

Further structural investigation of the synthesized particles was carried out by Raman spectroscopic analysis (Fig. 2(b)). Under excitation at 514.5 nm, two prominent peaks, corresponding to the D band and G band of carbon materials, appeared at 1370 cm^{-1} and 1587 cm^{-1}, respectively. A weak and broadened band at 2870 cm^{-1} (originating from the overlapping bands at ~2720 cm^{-1} (2D band) and ~2950 cm^{-1} (D + G band)) was also observed, which is a characteristic of high-nitrogen-content CDs within a carbon structure.[28,32,33] In addition to the peaks mentioned above, a weak Raman band near 700 cm^{-1} corresponding to the in-plane rotation of six-fold rings in carbon was also found, which evidently demonstrates that nitrogen was incorporated in the carbon films.[34] In the low Raman shift regime, the peak observed at ~135 cm^{-1} is attributed to the CdTe transverse optical (TO) mode of QDs.[35] In particular, the CdTe TO mode is shifted to a lower wavenumber by ~5 cm^{-1} relative to that of bulk CdTe crystal, which is reported at ~140 cm^{-1}. Overall, such a shift indicates the presence of photon localization due to quantum confinement effects and suggests that the expected CdTe QDs are indeed in place.[36]

Following the sonication and dispersion of the synthesized CdTe/N-CDs in ethanol, the UV-vis absorbance of the solution was measured. As shown in Fig. 2(c), two absorption peaks and an absorption shoulder are observed. The absorption peaks located at 235 nm and 242 nm are due to the π–π* electron transfer of carbon rings containing N. Additionally, the absorption shoulder at 288 nm is assigned to the n–π* transition.[37] One interesting fact is that the CdTe QD absorption peak at 540 nm is not observed in the spectrum of the CdTe/N-CDs. The fluorescent properties of the CdTe/N-CDs are displayed in Fig. 3. The PL spectra of the CdTe/N-CDs show two strong PL peaks centered at 405 nm and 429 nm as well as a PL shoulder at 456 nm in Fig. 3(a). No emission from the CdTe QDs (Fig. S1†) is observed, which is consistent with the absorption curves. The quenching of absorbance and emission of the CdTe QDs results from the electron transfer process between the CdTe QDs and N-CDs. It has been revealed previously that CDs can efficiently extract photo-excited electrons from semiconductor QDs (CdTe, CdS, *etc.*) before their recombination in hybrid structures of CDs and semiconductor QDs, thus quenching the absorption and emission of semiconductor QDs.[23,38,39] The quenching efficiency of CDs is one order of magnitude higher than that of gold.[40] A similar mechanism may be responsible for the quenching of the CdTe QDs in this study. Based on this transfer process, a possible PL transition scheme for the CdTe/N-CDs is illustrated as Fig. 3(c). Under photo-excitation, electrons in the ground state of the N-CDs and CdTe QDs absorb photons and then are transited to higher energy levels. The CdTe QDs' photo-excited electron–hole pairs are separated, and most electrons are injected into the N-CDs to leave holes in the CdTe QDs.[39] The excited electrons only rarely transit back to combine with the holes in the CdTe QDs, which is the reason why the CdTe

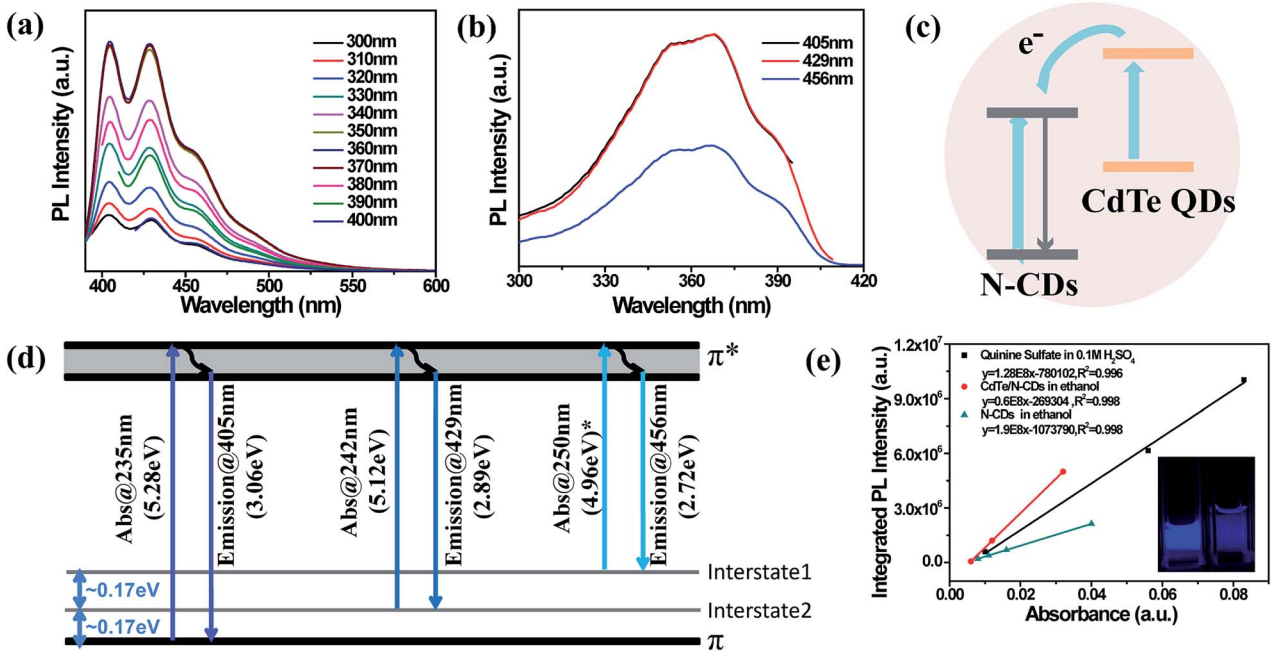

Fig. 3 (a) PL spectra of CdTe/N-CDs. The excitation wavelength ranges from 300 nm to 400 nm. (b) PLE spectra of CdTe/N-CDs. The emission wavelengths are 405 nm, 429 nm, 456 nm, respectively. (c) Photoluminescence transition scheme of CdTe/N-CDs. (d) Schematic diagram of the electronic transitions in the CdTe/N-CDs. *UV absorption peak at 250 nm was not detected. (e) Fluorescence quantum yield measurement results of quinine sulfate in 0.1 M H_2SO_4 solution, CdTe/N-CDs and N-CDs in ethanol. The excitation wavelength is 360 nm. The inset image is CdTe/N-CDs (left) and N-CDs (right) solution under the radiation of 370 nm light. The materials were sonicated and dispersed in ethanol.

QDs' absorption and emission are suppressed in the CdTe/N-CDs.

As the excitation wavelength increased from 300 nm to 400 nm, no detectable shift was noticed in terms of PL peak positions (Fig. 3(a)). The shapes of the emission curves also stayed unchanged, indicating that the fluorescent emission of the CdTe/N-CDs is independent of the excitation wavelength. Furthermore, the PL intensity reached its maximum in the excitation range of 360–380 nm, which is close to the intrinsic wavelength of GaN-based LEDs (3.4 eV).[41] Hence, the CdTe/N-CDs are of great potential in developing chip-based high performance optoelectronics devices by adopting a GaN LED as its excitation source. Regarding the PL excitation (PLE) spectra (Fig. 3(b)), a similar trend is observed. No shifts were observed for the peaks at 352 nm, 370 nm, and 390 nm when the excitation wavelength changed. Such excitation-independent emission and emission-independent excitation behaviours are ascribed to a uniform (either modified or passivated) surface state, and have also been observed in CDs,[42] graphene QDs[43] and N-CDs.[44,45] Hence, a uniform surface and its accordingly excitation-independent emission are expected to be the characteristics of our synthesized CdTe/N-CDs.

However, unlike common carbon materials with a single PL peak, whose intrinsic PL emission center is from the band gap of π-domain conjugation,[46] the three PL and PLE peaks of the CdTe/N-CDs are ascribed to three electron transition processes. The energy differences between the adjacent PL peaks (405, 429 and 456 nm) are 0.17 and 0.17 eV, and the energy differences between the adjacent PLE peaks (352, 370 and 390 nm) are likewise 0.17 and 0.17 eV. It is worth noting that a 0.17 eV energy difference is also equal to that between the two UV absorption peaks (235 and 242 nm) from the π–π* electron transfer.[47] It is probable that there are two interstates between the π and π* states, with energy levels 0.17 and 0.34 eV above the π energy level. A possible PL transition scheme of the CdTe/N-CDs is depicted as Fig. 3(d). Based on this hypothesis, there should be a UV absorption peak at 250 nm, which is 0.17 eV lower in energy than the peak at 242 nm. This peak, however, was not detected experimentally. Considering that the emission from π* to the second interstate (a shoulder at 456 nm) is quite weak compared to the other two emissions, and the electron transition probability is accordingly lower, the relevant absorption peak at 250 nm may be too weak to detect. It should be noted that the two interstates are different from surface trap states since the emissions are independent of the excitation wavelengths.

To explore the origin of the two interstates, pure N-CDs were prepared with only silk fibroin as the starting material for comparison. The TEM, XPS and Raman results of the pure N-CDs (Fig. S2–S4†) indicate a similar structure of the N-CDs to that of the N, CdTe-CD nanocomposites. The UV-vis absorption and PL spectra of the N-CDs (Fig. S5†) also exhibit similar peak positions and similar excitation-independent emission behaviour as that of the CdTe/N-CDs. It can be deduced that both the two interstates originate from the N-CDs and no extra states are introduced by the CdTe QDs. As the π–π* electron transfer originates from carbon rings containing N, it is reasonable to speculate that the π state and the two interstates may relate to

the three N-bonded configurations (pyridinic N, pyrrolic N and graphitic N) which were indicated in the XPS results.

To evaluate the optical properties of the CdTe/N-CDs, the QY and PL lifetime were studied. Fluorescence QY was measured with quinine sulfate (in 0.1 M H_2SO_4, QY ~54%) as a reference. As shown, the solution of CdTe/N-CDs exhibits much brighter blue-violet emission than the N-CDs under 370 nm radiation, and the QY of the N-CDs in ethanol is calculated to be 27% (Fig. 3(e)). For the hybridized CdTe QDs, the QY increased to about 84%, which was considerably higher than those of previously reported CDs.[48] Additionally, the QY and lifetime of the CdTe QDs have been studied, as illustrated in Fig. S6.† As the QYs of the CdTe QDs (53%) and N-CDs (27%) are both lower than that of the CdTe/N-CDs (84%), the fluorescence enhancement is presumably due to the interaction between the CdTe QDs and N-CDs rather than either of these two materials separately. Under excitation at 370 nm, the PL emission intensity is maximized with a Stokes-shift of 0.46 eV (370–429 nm). The transient PL spectrum of the CdTe/N-CDs (Fig. S7†) was well fitted with a two-exponential function, including two decay processes with lifetimes of $\tau_1 = 1.0$ ns (89.7% of the radiative emission) and $\tau_2 = 2.4$ ns (10.3% of the radiative emission), yielding an average PL decay time of $\tau =$ 1.0 ns (Table S1†). Generally, short lifetimes are attributed to the intrinsic recombination of PL centers while long lifetimes result from surface related emission.[49–51] The low proportion of the longer lifetime in the CdTe/N-CDs indicates that emission is mainly derived from the combination of intrinsic PL centers rather than from surface states, which is in agreement with the excitation-independent emission discussed above. As a comparison, the lifetimes of the N-CDs were fitted as $\tau_1 = 0.9$ ns (93.3% of the radiative emission) and $\tau_2 = 5.0$ ns (6.7% of the radiative emission), and average $\tau = 0.9$ ns. The short lifetime and its proportionality changed only slightly before and after hybridization, which is consistent with the similar PL behaviours of the CdTe/N-CDs and N-CDs. In contrast, the long lifetime is reduced by as much as half after hybridization, which may be attributed to the surface bonding between the N-CDs and CdTe QDs.

Based on the fitting data, the radiative rate constant (κ_r) and nonradiative rate constant (κ_{nr}) can be calculated using the equations of $\kappa_r = \varphi/\tau$ and $\kappa_{nr} = (1 - \varphi)/\tau$, respectively, where φ is the QY and τ is the average lifetime. It is found that the radiative rate constant increases from 3.0×10^8 s^{-1} to 8.4×10^8 s^{-1} after hybridization while the nonradiative rate constant decreases from 8.1×10^8 s^{-1} to 1.6×10^8 s^{-1} simultaneously. In accordance with the discussion above, the increased radiative rate constant and decreased nonradiative rate constant are ascribed to the CdTe QDs. As a large amount of photon-excited electrons transfer from the CdTe QDs to the N-CDs, the number of excited electrons in the N-CDs increases, accordingly improving the transition probability of the N-CDs from the excited state to the lower unoccupied state and in turn contributing to higher QY. Furthermore, unlike the simple mixture of N-CDs and CdTe QDs, which shows limited enhancement of N-CDs emission and incomplete quenching of CdTe QDs emission, the tight combination and hybridization in the CdTe/N-CDs make the electron transfer process more favorable and efficient. It is noteworthy that the CdTe/N-CDs were supported on carbon based nanosheets (as seen from the HRTEM image in Fig. 2 and wide characteristic 2D peak of the Raman spectrum). The nanosheets play a critical role in the electron transfer due to their ultra-high electrical conductivity.[55]

In this study, a QY of ~84% was obtained for the CdTe/N-CDs synthesized with a mixture of CdTe QDs and silk fibroin (SF) with a volume ratio of 1 : 1. The influences of the ratio of SF and CdTe QDs in the starting materials on the PL properties of the final sample are summarized in the ESI (see Fig. S9(a) and (b)†). Although the SF/CdTe QDs ratio varied, similar shapes and positions of peaks were observed on the fluorescence spectra for all ratios. In addition, the QY of the samples was found to be higher than that of pure N-CDs (Fig. S8(b)†). It was also observed that the QY reached the maximum of 84% when the SF/CdTe QDs ratio was 1 : 1 as described in the manuscript. Therefore, only the sample with the ratio 1 : 1 was chosen as the research subject and studied.

Experimental

Preparation

Thioglycolic acid (TGA) capped CdTe QDs were prepared first based on the reference method.[52] Briefly, a mixture of $CdCl_2$ and TGA was adjusted to pH 9.1 by using 1.0 mol L^{-1} NaOH solution, and then the mixture was aerated with N_2 for 30 min. After injection of freshly prepared NaHTe solution into the mixture, CdTe crude solution was obtained. The initial molar ratio of $CdCl_2$/TGA/NaHTe was 1.0/2.4/0.2 with the Cd^{2+} concentration being 1.0 mmol L^{-1}. Then the mixture was refluxed for 3 h to obtain CdTe QDs.

The other starting material for the preparation of CdTe/N-CDs was silk fibroin. Firstly, silk fibroin powders were dissolved in a 9.3 M LiBr aqueous solution at 60 °C for 4 h yielding a 20% (w/v) solution. Then, the solution was dialyzed in water using Slide-a-Lyzer dialysis cassettes for 48 h. The final concentration of the aqueous silk fibroin solution obtained was 6.57 wt%.

A copper substrate was cleaned, spin-coated with the mixture of CdTe QDs and silk fibroin with a volume ratio of 1 : 1, and then naturally dried in a Petri dish over 24 h. The dried Cu substrate was put into a home-build 2.45 GHz plasma reactor for plasma treatment. The plasma treatment conditions were set to be: microwave power at 850 W, pressure at 10 torr, nitrogen flow rate at 50 sccm, and treatment time for 30 min. Following the removal of the microwave power, the sample was cooled down to room temperature under the nitrogen flow of 30 sccm and the vacuum pressure at 15 torr. N-CDs were prepared under the same conditions, except using only silk fibroin as the starting material.

Characterization

The surface and composition study of the synthesized nanocomposites were carried using different spectroscopic methods. The XPS analysis with a binding energy of 284.8 eV

for the C 1s level as an internal reference was performed with a Kratos Axis Ultra DLD spectrometer employing an Al Kα monochromatized radiation as an X-ray source. The microstructural morphologies of the samples were examined by HRTEM (JEOL JEM2100). Raman scattering spectra were collected using a Renishaw confocal Raman spectroscope (Renishaw inVia, Gloucestershire GL12 7DW, United Kingdom) with a laser operating at 514.5 nm wavelength and 10 mW power output. The studied area on the sample surface was 2 μm in diameter.

To study the optical properties, the N-CDs and CdTe/N-CDs on the Cu substrate were immersed in ethanol and sonicated for 20 min. The UV-vis absorption spectrum of the resulting solution was recorded with a Shimadzu 3600 UV-vis near-infrared spectrophotometer. The fluorescence emission was measured by a Shimadzu RF-6000 spectrofluorimeter, and the lifetime spectrum was obtained in a FM-4P-TCSPC spectrofluorimeter. The excitation wavelength was 370 nm and the emission wavelength was 428 nm. All measurements were performed at room temperature.

Quantum yield measurements

Following a classic procedure obtained from the literature, quinine sulfate (in 0.1 M H_2SO_4 as solvent, with QY of 54%) was chosen as a ref. 53 and 54 The comparison between the integrated PL intensity and the absorbance values of the samples with those of the reference, referred to as the slope method, was used to determine the QY of the samples. The numerical value of the QY was calculated according to the equation: $\eta_x = \eta_{re}(K_x/K_{re})(n_x/n_{re})^2$, where η is the QY, K is the slope determined from the curves and n is the refractive index of the solvent. The subscripts re and x refer to the reference and the samples, respectively.

Conclusions

In summary, novel N doped carbon dots-CdTe QDs hybrid nanostructures with highly fluorescent properties have been synthesized in a single-step plasma heating process. Excitation-independent blue-violet emissions were observed from the CdTe/N-CDs hybrids in ethanol solvent. Unlike luminescence due to surface defects, which has uncontrollable emission, the intrinsic structure of the CdTe/N-CDs hybrids gives rise to fixed emission. The CdTe QDs provide additional excited electrons to the excited state of the N-CDs and improve the QY from 26% to 84%. Furthermore, the optimal excitation wavelength is found to be at 360–380 nm, which closely matches the intrinsic emission wavelength of GaN-based LEDs, showing potential in developing chip-based high performance optoelectronics devices.

Conflicts of interest

There are no conflicts to declare.

Acknowledgements

Authors thank the support from the National Natural Science Foundation of China (Grant No. 51702075).

Notes and references

1 H. Li, Z. Kang, Y. Liu and S. T. Lee, *J. Mater. Chem.*, 2012, **22**, 24230–24253.
2 X. Xu, R. Ray, Y. Gu, H. J. Ploehn, L. Gearheart, K. Raker and W. A. Scrivens, *J. Am. Chem. Soc.*, 2004, **126**, 12736–12737.
3 S. N. Polyakov, V. N. Denisov, B. N. Mavrin, A. N. Kirichenko, M. S. Kuznetsov, S. Y. Martyushov, S. A. Terentiev and V. D. Blank, *Nanoscale Res. Lett.*, 2016, **11**, 11.
4 Y.-Q. Zhang, D.-K. Ma, Y.-G. Zhang, W. Chen and S.-M. Huang, *Nano Energy*, 2013, **2**, 545–552.
5 S. T. Yang, L. Cao, P. G. Luo, F. Lu, X. Wang, H. Wang, M. J. Meziani, Y. Liu, G. Qi and Y. P. Sun, *J. Am. Chem. Soc.*, 2009, **131**, 11308–11309.
6 J. Tang, B. Kong, H. Wu, M. Xu, Y. Wang, Y. Wang, D. Zhao and G. Zheng, *Adv. Mater.*, 2013, **25**, 6569–6574.
7 H. Wang, Y. Wang, J. Guo, Y. Su, C. Sun, J. Zhao, H. Luo, X. Dai and G. Zou, *RSC Adv.*, 2015, **5**, 13036–13041.
8 Y. Wang, M. Wu, S. Yu and C. Jiang, *RSC Adv.*, 2018, **8**, 12708–12713.
9 S. Zhu, Q. Meng, L. Wang, J. Zhang, Y. Song, H. Jin, K. Zhang, H. Sun, H. Wang and B. Yang, *Angew. Chem., Int. Ed.*, 2013, **125**, 3953–3957.
10 Y. Wang, Y. Zhu, S. Yu and C. Jiang, *RSC Adv.*, 2017, **7**, 40973–40989.
11 H. Liu, T. Ye and C. Mao, *Angew. Chem., Int. Ed.*, 2007, **46**, 6473–6475.
12 Q.-L. Zhao, Z.-L. Zhang, B.-H. Huang, J. Peng, M. Zhang and D.-W. Pang, *Chem. Commun.*, 2008, **41**, 5116–5118.
13 Y.-P. Sun, B. Zhou, Y. Lin, W. Wang, K. A. S. Fernando, P. Pathak, M. J. Meziani, B. A. Harruff, X. Wang, H. Wang, P. G. Luo, H. Yang, M. E. Kose, B. Chen, L. M. Veca and S.-Y. Xie, *J. Am. Chem. Soc.*, 2006, **128**, 7756–7757.
14 S.-L. Hu, K.-Y. Niu, J. Sun, J. Yang, N.-Q. Zhao and X.-W. Du, *J. Mater. Chem.*, 2009, **19**, 484–488.
15 H. Zheng, Q. Wang, Y. Long, H. Zhang, X. Huang and R. Zhu, *Chem. Commun.*, 2011, **47**, 10650–10652.
16 H. Sun, L. Wu, N. Gao, J. Ren and X. Qu, *ACS Appl. Mater. Interfaces*, 2013, **5**, 1174–1179.
17 A. Cao, Z. Liu, S. Chu, M. Wu, Z. Ye, Z. Cai, Y. Chang, S. Wang, Q. Gong and Y. Liu, *Adv. Mater.*, 2010, **22**, 103–106.
18 D. I. Son, B. W. Kwon, D. H. Park, W. S. Seo, Y. Yi, B. Angadi, C. L. Lee and W. K. Choi, *Nat. Nanotechnol.*, 2012, **7**, 465.
19 Y. Wang, H. Li, J. Yao, X. Wang and M. Antonietti, *Chem. Sci.*, 2011, **2**, 446–450.
20 Y. Dai, H. Long, X. Wang, Y. Wang, Q. Gu, W. Jiang, Y. Wang, C. Li, T. H. Zeng and Y. Sun, *Part. Part. Syst. Charact.*, 2014, **31**, 597–604.
21 P. Anilkumar, X. Wang, L. Cao, S. Sahu, J.-H. Liu, P. Wang, K. Korch, K. N. Tackett Ii, A. Parenzan and Y.-P. Sun, *Nanoscale*, 2011, **3**, 2023–2027.

22 Y.-P. Sun, X. Wang, F. Lu, L. Cao, M. J. Meziani, P. G. Luo, L. Gu and L. M. Veca, *J. Phys. Chem. C*, 2008, **112**, 18295–18298.
23 X. Dai, H. Wang, Z. Qian, Q. Yi, Y. Wang, S. Cong, J. Zhao, Y. Sun, J. Huang, J. Xiong, H. Luo and G. Zou, *Appl. Phys. Lett.*, 2015, **107**, 203108.
24 Y. Wang, C. Zhang, X. Chen, B. Yang, L. Yang, C. Jiang and Z. Zhang, *Nanoscale*, 2016, **8**, 5977–5984.
25 S. Barman and M. Sadhukhan, *J. Mater. Chem.*, 2012, **22**, 21832–21837.
26 J. S. Lee, X. Wang, H. Luo and S. Dai, *Adv. Mater.*, 2010, **22**, 1004–1007.
27 T. V. Khai, G. N. Han, S. K. Dong, J. K. Yong, H. Ham, K. B. Shim and H. W. Kim, *J. Mater. Chem.*, 2012, **22**, 17992–18003.
28 H. Wang, T. Maiyalagan and X. Wang, *ACS Catal.*, 2012, **2**, 781–794.
29 Q. Liu, B. Guo, Z. Rao, B. Zhang and J. R. Gong, *Nano Lett.*, 2013, **13**, 2436–2441.
30 H. Ding, S.-B. Yu, J.-S. Wei and H.-M. Xiong, *ACS Nano*, 2016, **10**, 484–491.
31 H. Niu, L. Zhang, M. Gao and Y. Chen, *Langmuir*, 2005, **21**, 4205–4210.
32 R. Podila, J. Chacon-Torres, J. T. Spear and T. Pichler, *Appl. Phys. Lett.*, 2012, **101**, 389–4980.
33 K. N. Kudin, B. Ozbas, H. C. Schniepp, R. K. Prud'homme, I. A. Aksay and R. Car, *Nano Lett.*, 2008, **8**, 36–41.
34 A. Andreyev, M. Akaishi and D. Golberg, *Diamond Relat. Mater.*, 2002, **11**, 1885–1889.
35 O. R. Ochoa, E. J. W. Iii, C. Colajacomo, J. H. Simmons and B. G. P. Jr, *J. Mater. Sci. Lett.*, 1997, **16**, 613–616.
36 J. S. W. Mak, A. A. Farah, F. Chen and A. S. Helmy, *ACS Nano*, 2011, **5**, 3823–3830.
37 Z. Luo, Y. Lu, L. A. Somers and A. T. C. Johnson, *J. Am. Chem. Soc.*, 2009, **131**, 898.
38 Z. Chen, S. Berciaud, C. Nuckolls, T. F. Heinz and L. E. Brus, *ACS Nano*, 2010, **4**, 2964–2968.
39 S. Kaniyankandy, S. Rawalekar and H. N. Ghosh, *J. Phys. Chem. C*, 2012, **116**, 16271–16275.
40 A. Kasry, A. A. Ardakani, G. S. Tulevski, B. Menges, M. Copel and L. Vyklicky, *J. Phys. Chem. C*, 2012, **116**, 2858.
41 B.-J. Kim, G. Yang, H.-Y. Kim, K. H. Baik, M. A. Mastro, J. K. Hite, C. R. Eddy, F. Ren, S. J. Pearton and J. Kim, *Opt. Express*, 2013, **21**, 29025–29030.
42 X. Li, S. Zhang, S. A. Kulinich, Y. Liu and H. Zeng, *Sci. Rep.*, 2014, **4**, 4976.
43 Y. Dong, J. Shao, C. Chen, H. Li, R. Wang, Y. Chi, X. Lin and G. Chen, *Carbon*, 2012, **50**, 4738–4743.
44 D. Qu, M. Zheng, P. Du, Y. Zhou, L. Zhang, D. Li, H. Tan, Z. Zhao, Z. Xie and Z. Sun, *Nanoscale*, 2013, **5**, 12272–12277.
45 S. Zhang, J. Li, M. Zeng, J. Xu, X. Wang and W. Hu, *Nanoscale*, 2014, **6**, 4157–4162.
46 S. Zhu, Y. Song, X. Zhao, J. Shao, J. Zhang and B. Yang, *Nano Res.*, 2015, **8**, 355–381.
47 L. Tang, R. Ji, X. Cao, J. Lin, H. Jiang, X. Li, K. S. Teng, C. M. Luk, S. Zeng and J. Hao, *ACS Nano*, 2012, **6**, 5102.
48 A. J. Wang, H. Li, H. Huang, Z. Qian and J. J. Feng, *J. Mater. Chem. C*, 2016, **4**, 8146–8160.
49 X. Wang, L. Qu, J. Zhang, X. Peng and X. Min, *Nano Lett.*, 2003, **3**, 1103–1106.
50 K. Zhao, J. Li, H. Wang, J. Zhuang and W. Yang, *J. Phys. Chem. C*, 2007, **111**, 5618–5621.
51 L. Bao, Z. L. Zhang, Z. Q. Tian, L. Zhang, C. Liu, Y. Lin, B. Qi and D. W. Pang, *Adv. Mater.*, 2011, **23**, 5801–5806.
52 N. Gaponik, D. V. Talapin, A. L. Rogach, K. Hoppe, E. V. Shevchenko, A. Kornowski, E. Alexander and H. Weller, *J. Phys. Chem. B*, 2002, **106**, 7177.
53 M. Rong, X. Song, T. Zhao, Q. Yao, Y. Wang and X. Chen, *J. Mater. Chem. C*, 2015, **3**, 10916–10924.
54 X. Zhai, P. Zhang, C. Liu, T. Bai, W. Li, L. Dai and W. Liu, *Chem. Commun.*, 2012, **48**, 7955.
55 L. Zheng, H. Zheng, D. X. Huo, F. M. Wu, L. Shao, P. Zheng, Y. Jiang, X. Zheng, X. Qiu, Y. Liu and Y. Zhang, *Sci. Rep.*, 2018, **8**, 9248.